

The Impact of The IGM on High-Redshift Ly α Emission Lines

Mark Dijkstra^{1*}, Adam Lidz^{2†} and J. Stuart B. Wyithe^{1‡}

¹*School of Physics, University of Melbourne, Parkville, Victoria, 3010, Australia*

²*Astronomy Department, Harvard University, 60 Garden Street, Cambridge, MA 02138, USA*

16 May 2019

ABSTRACT

We calculate the impact of the intergalactic medium (IGM) on the observed Ly α lines emitted by galaxies in an ionised IGM at $z \geq 4$. Our model accounts for gas clumping in the IGM and for the fact that high-redshift galaxies reside in overdense regions, which causes the velocity field of the IGM to depart from the Hubble flow. The observed shape of the Ly α line varies widely, with dependence on the intrinsic width and systemic velocity of the line, a galaxies star formation rate and the local extra-galactic UV-background. For large star formation rates and levels of the UV-background, the Ly α line is not asymmetric as is common among known high-redshift Ly α emitters. For models in which the lines do show the observed strong asymmetry, the IGM typically transmits only 10–30% of the Ly α flux. The increase in the ionising background that accompanied the completion of reionisation barely increased the IGM transmission, which suggests that LAEs of comparable luminosity should not appear to be significantly dimmer prior to overlap. In this light, we briefly discuss the potential of Ly α emitters as a probe into the epoch of reionisation.

Key words: cosmology: theory—galaxies: high redshift—line: profiles—radiative transfer

1 INTRODUCTION

The Ly α emission line is a powerful tracer of young galaxies (Partridge & Peebles 1967) and quasars (e.g. Fan et al. 2006) in the high redshift universe. Since the discovery of the first high-redshift Ly α emitters (Steidel et al. 1996; Trager et al. 1997, hereafter, LAEs), existing Ly α surveys have detected several hundred galaxies out to redshift $z = 7.0$ (e.g. Hu et al. 1998; Rhoads et al. 2000; Malhotra & Rhoads 2002; Hu et al. 2002; Kodaira et al. 2003; Dawson et al. 2004; Stanway et al. 2004; Tran et al. 2004; Taniguchi et al. 2005; Westra et al. 2006; Tapken et al. 2006; Kashikawa et al. 2006; Shimasaku et al. 2006; Iye et al. 2006; Stanway et al. 2007), and the number of these known LAEs is steadily growing. The total flux in the Ly α line emerging from galaxies provides a measure of its star formation rate, while its exact shape contain information on the sources powering the emission and on the gas distribution and kinematics through which the Ly α photons propagate.

For example, the shape of the Ly α emission line as-

sociated with outflows produced by superwinds is typically peaked on a frequency redshifted by v_w relative to the true line center, where v_w is the speed of the outflowing gas. Furthermore, the spectrum is typically asymmetric and contains more photons redward of this peak (Ahn 2004; Hansen & Oh 2006; Tasitsiomi 2006; Verhamme et al. 2006). On the other hand, the Ly α emission line from galaxies surrounded by neutral collapsing gas clouds is expected to be blueshifted relative to the true line center, by an amount that depends on the infall velocity and the total column density of neutral hydrogen in the infalling gas (Zheng & Miralda-Escudé 2002; Tasitsiomi 2006; Dijkstra et al. 2006a; Verhamme et al. 2006).

It is well known that the total flux in the Ly α line and its shape are affected by subsequent scattering in the IGM. To first order, the IGM at high redshift erases the blue half, and transmits the red half of the line, reducing the total Ly α flux by a factor of 2. This is due to the fact that photons blueward of the Ly α transition will redshift into the Ly α resonance, where there is a large probability for the photon to be scattered out of the line of sight. Photons redward of the Ly α transition will redshift further and further away from resonance, which reduces the probability that these photons are scattered out of the line of sight. This simple picture would apply if the gas surrounding the galaxy is

* E-mail:dijkstra@physics.unimelb.edu.au

† E-mail:alidz@cfa.harvard.edu

‡ E-mail:swyithe@physics.unimelb.edu.au

expanding with the Hubble flow. However, infall of IGM gas onto galaxies will occur out to distances well beyond the virial radius (Loeb & Eisenstein 1995; Barkana 2004). Furthermore, this infalling gas is expected to be significantly overdense, with values as large as $\Delta \sim 20$ times the mean density (just outside the virial radius § 3).

Infall may have strong implications for the impact of the IGM on the Ly α emitted by galaxies. Santos (2004) has calculated the impact of an infalling neutral (i.e. pre-reionisation) IGM on a galaxies Ly α spectrum and found that the IGM typically erases a large fraction of the red side of the Ly α line. Therefore, much more than half of the Ly α is lost, with the IGM transmitting only $T_\alpha \sim 10^{-3} - 0.3$ of all Ly α photons. This low IGM transmission is partly due to the IGM damping wing, and partly due to resonant absorption by neutral hydrogen atoms in the infall region (see Fig. 8 of Santos 2004). Barkana & Loeb (2003) have found evidence for gas infall in the Ly α spectra of one bright quasar at $z = 4.8$. Despite its large ionising flux, denser clumps in the infalling gas absorb observable amounts of Ly α , reducing the total Ly α transmission well below 1. In addition, Dijkstra et al. (2006b) have shown that infall may also explain the observed spectrum of Steidel et al. (2000)'s Ly α 'Blob' LAB1 (Wilman et al. 2005) and the peculiar line shape of a $z = 5.8$ Ly α emitter observed by Bunker et al. (2003). These observations suggest that if infall is common around known LAEs, then their intrinsic Ly α luminosities, and consequently, their star-formation rates, may have been (significantly) underestimated in many cases, since the Ly α transmission is generally not corrected for infall.

In this paper we address the question: How does the IGM affect the shape and transmission of the Ly α emission line? Our approach is similar to the work of Santos (2004) and our results are consistent whenever there is overlap. However, we expand upon this work in several important ways: (1.) we incorporate gas clumping in the IGM; (2.) we investigate the impact of clustering of galaxies on the IGM transmission; (3.) we calculate the skewness parameter, S_W , which was recently introduced by Kashikawa et al. (2006). However, the biggest difference between this paper and previous work is our focus on the reionised IGM: although it is generally understood that a neutral IGM can strongly suppress Ly α emission from galaxies (Gunn & Peterson 1965; Haiman 2002; Santos 2004), the impact of an ionised IGM has been virtually ignored. As discussed in § 5.5 our analysis is also relevant in scenarios in which large disjoint HII bubbles exist prior to the end of reionisation (Furlanetto et al. 2004a; Wyithe & Loeb 2004). Note that we focus on the Ly α line emitted by galaxies. For a brief discussion on the impact of the IGM on Ly α lines emitted by quasars, the reader is referred to Dijkstra & Wyithe (2006). The outline of this paper is as follows: We review the mechanism that creates Ly α emission in star forming galaxies, and discuss its expected properties in § 2. We describe our model for the IGM in § 3. In § 4 we present calculations of the modified shape of the Ly α line. We discuss various implications of our results in § 5, before presenting conclusions in § 6. The parameters for the background cosmology used throughout this paper are $\Omega_m = 0.24$, $\Omega_\Lambda = 0.76$, $\Omega_b = 0.044$, $h = 0.73$ and $\sigma_8 = 0.74$ (Spergel et al. 2006).

2 LY α EMISSION FROM STAR FORMING GALAXIES

2.1 The Ly α Luminosity vs. Star Formation Rate

In this section we review the relation between the star formation rate in galaxies and Ly α luminosity, and discuss its uncertainties. The Ly α flux from star forming galaxies originates in the dense nebulae from which the stars form. Ionising photons produced by O stars, which are absorbed in the nebulae, are converted into Ly α in about 2 out of 3 cases (Osterbrock 1989, for case-B recombination, p 367). Under the assumption that all Ly α photons escape from the galaxy into the IGM (sometimes referred to as the 'dust-uncorrected' Ly α luminosity), the total Ly α luminosity of a galaxy can then be estimated from

$$L_{\text{Ly}\alpha} = 0.68h\nu_\alpha[1 - f_{\text{esc}}]\dot{Q}_H, \quad (1)$$

where $h\nu_\alpha = 10.2$ eV is the energy of a Ly α photon, f_{esc} is the escape fraction of ionising photons, and \dot{Q}_H is total luminosity of ionising photons. As \dot{Q}_H depends on the number of O-stars, its value depends on the assumed IMF and metallicity of the gas from which the stars form. Under the assumption of constant star formation rate (as opposed to a star burst), Schaerer (2003) has calculated \dot{Q}_H for several different IMFs, and for a range of metallicities Z (expressed in solar units Z_\odot). For a Salpeter IMF with lower and upper mass limits of $M_l = M_\odot$ and $M_u = 100M_\odot$, respectively

$$\log_{10} \dot{Q}_H = 53.8 + \log_{10} \dot{M}_* - 0.0029(9 + \log_{10} Z)^{2.5}, \quad (2)$$

in which \dot{M}_* is the star formation rate in M_\odot/yr . Schaerer (2003) also calculates the time-evolution of \dot{Q}_H for an instantaneous star burst. In this case, \dot{Q}_H can be very high, reaching values of $\log_{10} \dot{Q}_H(\text{photons s}^{-1} M_\odot^{-1}) \sim 47 - 48$, during the first few Myr after the star burst. For the remainder of this paper, we will assume the star formation does not take place in such a burst and we will use Eq (1) and Eq (2) to calculate $L_{\text{Ly}\alpha}$ as a function of \dot{M}_* . Following Santos (2004), our models assume $f_{\text{esc}} = 0.1$ (Inoue et al. 2006) and $Z = 0.05Z_\odot$, unless stated otherwise.¹ This low metallicity reflects that galaxies at $z \gtrsim 4 - 5$ live in universe that is $\lesssim 1$ Gyr old, and in which there has been less time for their gas to become enriched by metals and dust.

2.2 The Shape+Width of the Intrinsic Ly α Line

For simplicity, the shape of the intrinsic Ly α line is usually assumed to be Gaussian. For gas that is optically thin to Ly α photons, a reasonable choice for the standard deviation of this Gaussian emission line is $\sigma_\alpha \sim 1.5v_{\text{circ}}$ (Santos 2004). However, to take this value for all galaxies assumes that each star forming, Ly α emitting galaxy is a disk seen edge-on, which is only true for a small subset of LAEs. For disk

¹ For comparison, given solar metallicities ($Z = Z_\odot$) the total output of ionising photons is related to the star formation rate through $\log_{10} \dot{Q}_H = 53.0 + \log_{10} \dot{M}_*$ (Kennicutt 1998). This relation is often used in the literature and is a lower by factor of 2 than the relation used in this paper. The uncertainties in the relation between $L_{\text{Ly}\alpha}$ and \dot{M}_* introduced by the gas metallicity and by the IMF are ignored for the remainder of this paper. Here, our focus is on the uncertainties introduced by the IGM.

galaxies seen face-on, the Ly α line is narrower. To account for this inclination effect, the fiducial intrinsic Ly α emission line should be lowered to $\sigma_\alpha \sim 0.7 \times 1.5v_{\text{circ}} \approx v_{\text{circ}}$ (where $\langle |\cos i| \rangle \sim 0.7$, and i is inclination angle of the galaxy).

As already mentioned, the previous discussion applies when the gas inside the galaxy is optically thin to Ly α photons. Since the line-center Ly α optical depth exceeds unity for hydrogen columns $N_H \gtrsim 10^{13} \text{ cm}^{-2}$, the optically thin approximation is most likely incorrect. Indeed, as mentioned in § 5.1 the bulk of Ly α photons are believed to be emitted inside dense nebulae in which star formation is occurring. For ionising photons to be converted into Ly α , these nebulae must be optically thick to ionising radiation. This requires hydrogen to have a column of $N_H \gtrsim 10^{17} \text{ cm}^{-2}$, making the line center Ly α optical depth $\tau_0 \gtrsim 10^4$. Resonant scattering of Ly α photons through optically thick neutral hydrogen gas clouds may boost the width of the Ly α emission line. However, resonant scattering is not expected to boost the Ly α line width significantly.

For example, if we have Ly α photons emitted in the center of a static uniform slab/sphere with line-center optical depth τ_0 , then resonant scattering causes the emerging spectrum to comprise two peaks, each separated from the line center by $\sim 180(N_H/10^{20} \text{ cm}^{-2})^{1/3}(T_{\text{gas}}/10^4 \text{ K})^{1/6} \text{ km s}^{-1}$, where T_{gas} is the gas temperature (Harrington 1973; Neufeld 1990; Dijkstra et al. 2006a). The FWHM of the resonant profile is ~ 2.5 times as large as this separation.

To quantify the impact of resonant scattering on the width of the line, we convolve a Gaussian emission line with the resonant profile derived by Harrington (1973) and Neufeld (1990). For this example, the Gaussian has a standard deviation of $v_{\text{circ}} = 160 \text{ km s}^{-1}$. The associated physical picture is that Ly α photons emerge from the nebula in which they were created with a double peaked emission spectrum, after which they can freely escape from the galaxy. For simplicity, we assume that the total column of hydrogen, N_H , is the same for each nebula. In Figure 1 we show Ly α emission lines for various values of N_H . The figure shows that broadening of the line is not important for $N_H \lesssim 10^{20} \text{ cm}^{-2}$. The main reason is that in this example, the FWHM of the Gaussian is comparable to the FWHM of the resonant profile for $N_H = 10^{20} \text{ cm}^{-2}$, which is $\sim 450 \text{ km s}^{-1}$. For larger columns the Ly α line broadens and displays the double-peak of the resonant profile.

The column densities of atomic hydrogen observed in local galaxies typically lie in the range $N_H = 10^{20} - 10^{21} \text{ cm}^{-2}$ (e.g. Bosma 1981; Kunth et al. 1998), but may reach larger values. This suggests that resonant scattering can boost the observed Ly α widths significantly. However, the above calculation represents an upper limit on the amount of resonant broadening for a given N_H , because the calculation assumed the hydrogen gas to be uniform and static. In reality, velocity gradients in the gas will facilitate the escape of Ly α from the nebula, resulting in a reduced broadening through resonant scattering. Furthermore, the observation that ionising radiation does emerge from star forming regions suggests that paths through the galaxy must exist along which $N_H \lesssim 10^{17} \text{ cm}^{-2}$. If Ly α photons escape through these lower column-density paths, then resonant broadening of the Ly α line is negligible. This also applies when the ISM consists of two phases in which case

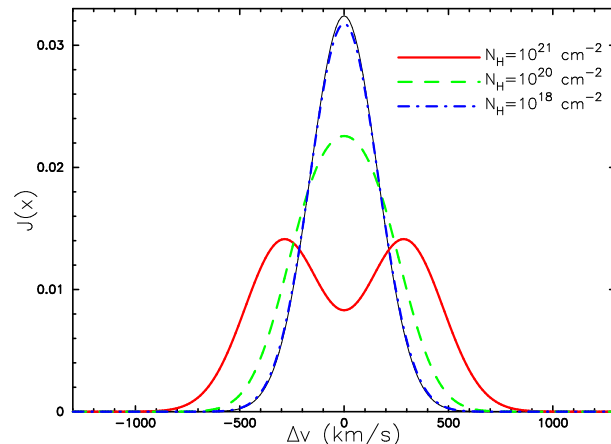


Figure 1. Broadening of the Ly α emission line through resonant scattering. The Ly α flux density $J(x)$ (arbitrary units) is shown as a function of velocity off-set from the true line center. A Gaussian Ly α emission line with $\sigma_v = 160 \text{ km s}^{-1}$, was convolved with the 'resonant profile', which is the line profile that would emerge from a static, uniform slab with a hydrogen column density N_H (see text). When $N_H \gtrsim 10^{20} \text{ cm}^{-2}$, resonant scattering of the Ly α emission line becomes more important.

resonant scattering is even less important (see § 2.3). The possibility that the majority of Ly α photons escape through these 'low column density paths', has been invoked as an explanation that the Ly α photons manage to escape from galaxies at all (e.g Neufeld 1991; Kunth et al. 1998).

We conclude that resonant scattering of Ly α photons is not expected to broaden the width of the Ly α emission line of galaxies with $v_{\text{circ}} \gtrsim 150 - 200 \text{ km s}^{-1}$ by a factor $\gtrsim 2$. For significantly less massive galaxies, i.e. $v_{\text{circ}} \lesssim 50 \text{ km s}^{-1}$, resonant scattering could in principle broaden the line to a few hundred km s^{-1} (since this requires columns of only $N_H \sim 10^{20} \text{ cm}^{-2}$) though it may not if the Ly α escapes through 'low column density paths'.

2.3 The Equivalent Width of the Ly α Line

If we approximate the spectrum of a source blueward of the Ly α frequency using a powerlaw of the form $f_\nu = k\nu^\beta$, then the maximum intrinsic Ly α EW is given by (Charlot & Fall 1993, for $\beta < -1$)

$$\text{EW}_{\text{max}} = \frac{0.68h\nu_\alpha \int_{\nu_H}^{\infty} \frac{f(\nu)}{h\nu} d\nu}{f_\lambda(\lambda = \lambda_\alpha)} = -0.68 \frac{\lambda_\alpha}{\beta} \left(\frac{\nu_H}{\nu_\alpha} \right)^\beta, \quad (3)$$

where $h = 6.62 \times 10^{-27} \text{ erg s}$, is Planck's constant and $\nu_H = 3.28 \times 10^{15} \text{ Hz}$, is the hydrogen ionisation threshold. The Ly α flux was calculated assuming that two-thirds of all ionising photons are converted into Ly α , i.e. we assumed the escape fraction of ionising photons to be $f_{\text{esc}} = 0$. EW_{max} is then obtained after dividing this number by the continuum flux density (in $\text{erg s}^{-1} \text{ \AA}^{-1}$) at the Ly α frequency. Here, we used the relation $\lambda f_\lambda = \nu f_\nu$ and have denoted the Lyman limit frequency with ν_H . For stars, the index β is typically -4 to -5 and we get that $\text{EW}_{\text{max}} = 64 \text{ \AA}$ (for $\beta = -4$). Charlot & Fall (1993) showed, using stellar synthesis models in combination with realistic stellar spectra,

that the maximum EW that is reached in the first $\sim 10^7$ yrs after the onset of star formation and can be as high as $\text{EW}_{\text{max}} \sim 300 \text{ \AA}$, although the precise value depends on the assumed IMF (e.g. Schaefer 2003).

Resonant scattering of Ly α photons increases the total distance traveled before the photons emerge from the galaxy. Therefore, Ly α is more subject to dust attenuation than the continuum photons, which can result in a reduction of the Ly α EW. However, the opposite may be true in a multi-phase ISM (Neufeld 1991; Hansen & Oh 2006), in which case the dust is locked up in cold clumps embedded in a hot ionised medium. The Ly α photons can escape from the galaxy scattering off the dust clumps, while mainly traveling through the ionised interclump medium. Depending on the details of clump size, clump dust content, etc, the fraction of Ly α transmitted through the ISM could exceed that of continuum photons. Therefore, the intrinsic Ly α EW produced by a normal stellar population could, in some cases, be larger than 300 \AA .

3 MODELING THE INTERGALACTIC MEDIUM

Our approach to modeling the IGM is based on Barkana (2004) who calculated the average density and velocity profiles of intergalactic gas around virialised halos of various masses. It is worth emphasising that infall of gas onto galaxies is inherent in the Press-Schechter model for the collapse of cold dark matter halos. This model is described below.

3.1 The IGM Density and Velocity Field

Figures 2 and 4 of Barkana (2004) show the average radial density and velocity profile of the intergalactic gas beyond the virial radius r_{vir} of objects of mass M_{tot} at various redshifts. Here, we focus on the density profile associated with $z = 5$ and $M_{\text{tot}} = 10^{10} M_{\odot} - 10^{12} M_{\odot}$. Just outside the virial radius, the average density, $\rho(r)$ is $\rho(r_{\text{vir}}) = 20\bar{\rho}$, where $\bar{\rho}$ is the mean baryon density of the universe. The density drops off approximately following a power-law $\rho(r) \propto r^{-1}$, and reaches a value of $\rho(r = 10r_{\text{vir}}) = 2\bar{\rho}$. At larger radii, the density asymptotically approaches $\bar{\rho}$ (see Fig 2 of Barkana, 2004). The velocity profile (Fig 4 of Barkana, 2004), shows the IGM to be collapsing at $\sim v_{\text{circ}}$, just outside the virial radius. The IGM is stationary with respect to the galaxy at $r \sim 5r_{\text{vir}}$. In this model, the IGM never becomes fully comoving, which is not surprising since the average density within a sphere of radius r is always larger than $\bar{\rho}$. The model should therefore break down beyond a certain radius. In this paper, we assume that this model applies up to $10r_{\text{vir}}$. Beyond this radius, we assume the IGM is simply comoving and at the mean density in the universe. To summarise, our fiducial IGM density and velocity fields are given by

$$\rho(r) = \begin{cases} 20\bar{\rho}(r/r_{\text{vir}}) & r < 10r_{\text{vir}}; \\ \bar{\rho} & r \geq 10r_{\text{vir}} \end{cases} \quad (4)$$

$$v_{\text{IGM}}(r) = \begin{cases} -v_{\text{circ}} + \frac{r}{10r_{\text{vir}}}(H(z)r + v_{\text{circ}}) & r < 10r_{\text{vir}}; \\ H(z)r & r \geq 10r_{\text{vir}}, \end{cases}$$

where $H(z)$ is the Hubble constant at redshift z .

3.2 Photoionisation of the IGM

If the galaxy spectrum is of the form $J(\nu) \propto \nu^{\beta}$ blueward of the hydrogen ionisation threshold, ν_H , then the total photoionisation rate at distance r from the galaxy is

$$\Gamma_{\text{ion}} = B_c(r)\Gamma_{\text{BG}} + \frac{\beta}{\beta - 3} \frac{\sigma_0 \dot{Q}_H f_{\text{esc}}}{4\pi r^2}, \quad (5)$$

where we approximate the hydrogen photoionisation cross section as $\sigma_H(\nu) = \sigma_0(\nu/\nu_H)^{-3}$, in which $\sigma_0 = 6.3 \times 10^{-18} \text{ cm}^{-2}$. The photoionisation rate due the extra-galactic background, Γ_{BG} , has been determined observationally to be $\sim 10^{-13} \text{ s}^{-1}$ between $z = 5$ and $z = 6$ (Fan et al. 2006). The factor $B_c(r)$ is the (radius dependent) boost in the ionising background due to the clustering of surrounding galaxies. Clustering is ignored in our fiducial model, i.e. $B_c(r) = 1$, but may be as large as 10^2 (see § 3.3). For a given Γ_{ion} , the neutral fraction of hydrogen is calculated from

$$x_H = 1 + \frac{\Gamma_{\text{ion}}}{2n_H \alpha_{\text{rec}}} - \left[\frac{\Gamma_{\text{ion}}}{n_H \alpha_{\text{rec}}} + \left(\frac{\Gamma_{\text{ion}}}{2n_H \alpha_{\text{rec}}} \right)^2 \right]^{1/2} \quad (6)$$

which was derived assuming photoionisation equilibrium and ignoring helium. Here, n_H is the number density of hydrogen nuclei and the case-A recombination coefficient $\alpha_{\text{rec}} = 4.2 \times 10^{-13} (T_{\text{gas}}/10^4 \text{ K})^{0.7} \text{ s}^{-1}$ (e.g. Hui & Gnedin 1997). We have verified that the total optical depth to ionising radiation is negligible in our calculations. We note that our optically-thin approximation is invalid if a dense, self-shielded and optically thick Lyman-limit system (LLs) lies along a given sightline. If anything, the presence of LLs would lower the actual photoionisation rate, which would increase the neutral fraction of hydrogen, which would in turn lower the overall Ly α transmission.

3.3 The Impact of Clustering of Sources on the Ionising Background

We have calculated the enhancement of the ionising background due to clustering of nearby galaxies using a semi-analytic model based on that described in Wyithe & Loeb (2005). Details of the model can be found in Appendix A, and we summarise only its main features here. We define a mean free path of ionising photons by λ , which we assume to be independent of radius. At a distance r from the central galaxy, this flux may be written as

$$F_{\text{bg}}(r) = \int d^3x \frac{\frac{dN}{dt}(|\vec{x}|)}{4\pi |\vec{r} - \vec{x}|^2} \exp \left[-\frac{|\vec{r} - \vec{x}|}{\lambda} \right], \quad (7)$$

where $dN/dt(r)$ gives the ionising photon production rate per unit volume from sources surrounding the central galaxy at radius r . The model computes $dN/dt(r)$ using a radius dependent mass function for galaxies in the infall-region. More details are given in Appendix A (Eq A1). Note that several model assumptions enter the expression of $dN/dt(r)$, which introduces some uncertainty into the exact enhancement of the background flux. However, the main purpose of this calculation, is to show that the boost in the ionising background is large (this statement is independent of the detailed model assumptions).

The resulting ionising background is shown in Figure 2 for the cases in which the central galaxy sits in

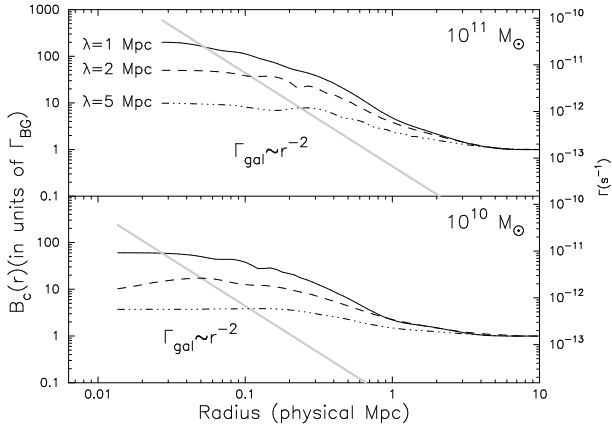


Figure 2. The boost in the ionising background $B_c(r)$ due to clustered sources surrounding the central galaxy for the cases $M_{\text{tot}} = 10^{11} M_\odot$ (top panel) and $M_{\text{tot}} = 10^{10} M_\odot$ (bottom panel). The boost is shown for 3 values of the assumed mean free path of the ionising photons (text). The vertical axis on the right shows the associated physical photoionisation rate (in s^{-1}). For comparison, the photoionisation rate due to the central galaxy is shown as the thick grey line for $\dot{M}_* = 10^2 M_\odot/\text{yr}$ (top panel) and $\dot{M}_* = 10 M_\odot/\text{yr}$ (bottom panel) also in units of the measured Γ_{BG}). For both cases, $B_c(r) \rightarrow 10^2$ when $\lambda \lesssim 2$ Mpc. Clustering of sources may boost the ionising background significantly. As a result, the total photoionisation rate is not dominated by the central galaxy beyond a few virial radii.

dark matter halos of mass $M_{\text{tot}} = 10^{11} M_\odot$ (top panel) and $M_{\text{tot}} = 10^{10} M_\odot$ (bottom panel). The flux $F_{\text{bg}}(r)$ is written in units of the mean background flux [i.e. we have plotted $B_c(r)$, Eq (5)]. To show the dependence of the boost on the assumed λ , $B_c(r)$ is shown for $\lambda = 1, 2$ and 5 physical Mpc, which covers the range of λ derived by Fan et al. (2006). Note that $B_c(r) \rightarrow 10^2$ for $\lambda \leq 2$ Mpc in both cases. For comparison, the ionising flux from the central galaxy is shown as the thick grey line for $\dot{M}_* = 10^2 M_\odot/\text{yr}$ (top panel) and $\dot{M}_* = 10 M_\odot/\text{yr}$ (bottom panel, more precisely, $\Gamma_{\text{gal}}/\Gamma_{\text{BG}}$ is shown, see Eq 5). In all cases, the total ionising flux is not dominated by that of the central galaxy beyond a few virial radii. The impact of this enhancement on the Ly α line is discussed in § 4.1.

3.4 The IGM Transmission

The total opacity seen by a photon initially at frequency ν is

$$\tau(\nu) = \sigma_0 \int_{r_{\text{vir}}}^{\infty} ds n_H(s) x_H(s) \phi\left(x(\nu) - \frac{v_{\text{IGM}}(s)}{v_{\text{th}}}\right), \quad (8)$$

where we denoted frequency in units of the dimensionless variable $x \equiv (\nu - \nu_\alpha)/\Delta\nu_D$, in which $\nu_D = \nu_\alpha(v_{\text{th}}/c)$; $v_{\text{th}} = (2kT_{\text{gas}}/m_p)^{1/2}$ is the thermal speed of atoms in the gas at temperature T_{gas} . We assume the gas temperature to be $T_{\text{gas}} = 10^4$ K, which is appropriate for the photoionised IGM. Note that the temperature of the IGM may actually have been as high as $T_{\text{gas}} = 5 \times 10^4$ K shortly after reionisation was completed (e.g. Hui & Hauman 2003). However, we found that our results are practically insensitive to the precise value of T_{gas} . The Ly α absorption cross section is written as $\sigma(x) = \sigma_0 \phi(x)$, where $\sigma_0 =$

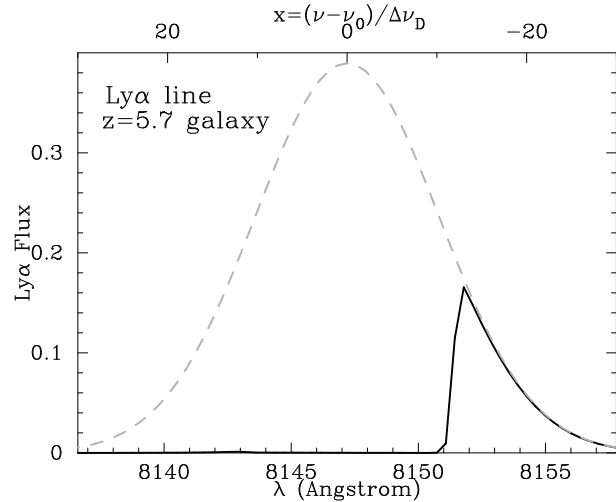


Figure 3. The impact of a post-reionisation i.e. fully ionised IGM on the observed shape of Ly α emission line emitted by a $z = 5.7$ star forming galaxy ($M_* = 10 M_\odot/\text{yr}$) in a dark matter halo with a mass of $M_{\text{tot}} = 10^{11} M_\odot$ (this mass is relevant for the extent of the infall region). The intrinsic shape (dashed line) of the Ly α line is Gaussian. The solid represents the observed shape after IGM processing. Here, only $\sim 12\%$ of the Ly α is transmitted to the observer.

$5.67 \times 10^{-14} (T_{\text{gas}}/10^4 \text{ K})^{-1/2} \text{ cm}^2$ and $\phi(x)$ is given by

$$\phi(x) = \begin{cases} \sim e^{-x^2} & \text{core;} \\ \sim \frac{a}{\sqrt{\pi x^2}} & \text{wing,} \end{cases} \quad (9)$$

The gas density profile $n_H(r)$ given by Eq (4), is azimuthally averaged. In reality, for a given line of sight, the density fluctuates around this average. These density fluctuations can cause significant deviations from the opacity calculated from Eq (8). If the density fluctuations are characterised by a distribution $P(\Delta)d\Delta$, which gives the probability that the gas density at radius r is in the range $\rho(r)[\Delta \pm d\Delta/2]$ (where $\rho(r)$ is given by Eq 4), then the average IGM transmission at frequency x

$$\langle e^{-\tau} \rangle(x) = \int_0^{\Delta_{\text{max}}} d\Delta P(\Delta) e^{-\Delta^2 \tau(x)}. \quad (10)$$

This equation is equivalent to Eq (9) in Barkana & Loeb (2004). Here, we take $\Delta_{\text{max}} = 100$, but note that the results presented depend very weakly on its value. The function $P(\Delta)d\Delta$ is not well known. Following Barkana & Loeb (2004) we take the distribution $P(\Delta)d\Delta$ derived by Miralda-Escudé et al. (2000), who obtained this distribution at various redshifts from a simulation. This means that the density fluctuations in the overdense regions are assumed to be the same as those at mean density.

Since $\phi(x)$ is peaked strongly around $x = 0$, Eq (8) states that the largest contribution to $\tau(x)$ comes from gas that resonates with the photons at this frequency. By combining Eq (5), Eq (6) and Eq (8) we can calculate the impact of the IGM on the Ly α emission line.

4 RESULTS

Our fiducial model consists of a star forming galaxy embedded in a dark matter halo with a total mass of $M_{\text{tot}} =$

$10^{11} M_\odot$. At $z = 5.7$, the halos' associated virial radius and circular velocity are 23 kpc and 133 km s^{-1} , respectively. The value of M_{tot} is chosen to facilitate comparison with Santos (2004). However, this choice of M_{tot} may be justified by the observed bias and clustering of high-redshift LAEs which suggest $M_{\text{tot}} = 10^{11} - 10^{13} M_\odot$ (Ouchi 2003). Furthermore, Wyithe & Loeb (2006) have recently presented a simple model which reproduces the observed Ly α luminosity function of Kashikawa et al. (2006). In their model, the observed LAEs have $M_{\text{tot}} = 10^{10} - 10^{11} M_\odot$. Using detailed semi-analytic galaxy formation models Le Delliou et al. (2006) found the typical halo mass of the observed LAEs to be $M_{\text{tot}} \sim 10^{11} M_\odot$. For the important results presented in this paper, our analysis is repeated for the case $M_{\text{tot}} = 10^{10} M_\odot$. For larger M_{tot} , the infall region is more extended and the IGM transmission is expected to be (even) lower. We assumed a star formation rate of $\dot{M}_* = 10 M_\odot/\text{yr}$, and the escape fraction of ionising photons to be $f_{\text{esc}} = 0.1$. The spectrum of the galaxy is of the form $J(\nu) \propto \nu^\beta$, where $\beta = -4.5$, for $\nu \geq \nu_H$ (§ 2.3). The impact of clustered sources on the ionising background is discussed later [here, $B_c(r) = 1$, Eq 5]. According to Eq (1-2), this galaxy has an intrinsic Ly α luminosity of $L_{\text{Ly}\alpha} = 2 \times 10^{43} \text{ erg s}^{-1}$.

In Figure 3 we show the shape of the Ly α line after it has been processed by the IGM. The *solid/dashed lines* show the observed/intrinsic Ly α spectrum, respectively. As discussed in § 1, the blue side of the line ($x > 0$) is suppressed significantly by the IGM. However, the suppression extends into the red part of the line. This is because of resonant absorption by residual neutral hydrogen gas that is falling onto the galaxy. The peak of the observed spectrum is redshifted relative to the true line center by an amount set by the infall velocity. Here, the redshift is $v_{\text{IGM}}(r_{\text{vir}}) = -v_{\text{circ}}$.

We denote the flux density in the Ly α line by $J(x)$, where x is the dimensionless frequency variable introduced in § 3.4. The total transmission is then given by

$$\mathcal{T}_\alpha \equiv \frac{\int_{-\infty}^{\infty} dx J(x) \langle e^{-\tau} \rangle(x)}{\int_{-\infty}^{\infty} dx J(x)}, \quad (11)$$

where $\langle e^{-\tau} \rangle(x)$ is given by Eq (10). For the example shown in Figure 3, $\mathcal{T}_\alpha = 0.12$, i.e. only 12% of the flux that emerges from the galaxy is transmitted through the IGM. The total observed flux of this galaxy is then $\mathcal{T}_\alpha \times L_{\text{Ly}\alpha} / [4\pi d_L^2(z)] = 6 \times 10^{-18} \text{ erg s}^{-1} \text{ cm}^{-2}$.

The exact shape of the observed Ly α line and the total transmitted flux depends on several other parameters, such as the assumed width of the intrinsic width of the Ly α line; the total ionising luminosity of the galaxy; the value of the ionising background etc. The variation in observable Ly α properties with these, and other parameters is studied next.

4.1 Variation of the Line Shape

In Figure 4 we show the impact of various parameters on the shape of the Ly α line after processing through the IGM. The IGM transmission for each curve is shown as a label. Also shown is the 'skewness parameter', S_W (Kashikawa et al.

2006)². This parameter quantifies the asymmetry of an emission line, which can be used to separate high redshift LAEs from lower redshift interlopers. This separation is possible as absorption in the IGM causes high redshift Ly α emission lines typically to be asymmetric (with a positive/negative skewness when the spectrum is shown as a function of wavelength/frequency, respectively), while lower redshift H α , [OIII] or [OII] emitters are not. Kashikawa et al. (2006); Shimasaku et al. (2006) found that the requirement $S_W \geq 3 \text{ \AA}$ can effectively distinguish between the two populations. Calculating S_W for our models is not trivial. The largest contribution to the skewness comes from pixels that lie far from the observed Ly α peak flux, and we found that the precise value of S_W depends somewhat on the assumed flux threshold, f_{min} , below which the Ly α line is lost in the noise. In particular, a very low level of residual flux on the blue side of the Ly α line can cause S_W to be negative for some of our models. To account for the dependence of S_W on f_{min} , we have shown the values of S_W we found for each model for the range $0.01f_{\text{max}} \leq f_{\text{min}} \leq 0.1f_{\text{max}}$, where f_{max} is the observed peak Ly α flux density.

- *Top Left:* Variation of \dot{M}_* : Here, we have plotted the cases $\dot{M}_* = 10 M_\odot/\text{yr}$ (black), $\dot{M}_* = 10^2 M_\odot/\text{yr}$ (grey) and $\dot{M}_* = 10^3 M_\odot/\text{yr}$ (red). Increasing \dot{M}_* results in a higher output of ionising photons which reduces the neutral fraction in the infall region, and allows more flux, both red and blueward of the line, to be transmitted. Note that for $\dot{M}_* \geq 100 M_\odot/\text{yr}$ $S_W < 3 \text{ \AA}$ in difference to known high-redshift LAEs. For $\dot{M}_* = 10^2 M_\odot/\text{yr}$ the spectrum shows a long tail on the blue side of the line, which makes S_W negative. On the other hand, for $\dot{M}_* = 10^3 M_\odot/\text{yr}$ the spectrum becomes practically symmetric with a skewness parameter $-0.7 \lesssim S_W \lesssim 0.5 \text{ \AA}$. The precise value of \dot{M}_* at which S_W becomes less than 3 \AA depends on the size of the infall region, and therefore on M_{tot} . For example, given $M_{\text{tot}} = 10^{10} M_\odot$, $S_W \lesssim 3 \text{ \AA}$ for $\dot{M}_* \gtrsim 10 M_\odot/\text{yr}$.

- *Top Right:* Variation of the width of the intrinsic Ly α line: $\sigma_\alpha = 1.0v_{\text{circ}}$ (black), $\sigma_\alpha = 0.7v_{\text{circ}}$ (red) and $\sigma_\alpha = 1.5v_{\text{circ}}$ (grey). Clearly, increasing σ_α increases \mathcal{T}_α , because a larger fraction of photons lie redward of the wavelength range affected by the infalling gas. Furthermore, the sharp break in the profile becomes more prominent towards larger σ_α .

- *Lower Left:* Variation of the ionising background Γ_{BG} : We show cases in which the ionising background is Γ_{BG} (black), $10\Gamma_{\text{BG}}$ (grey) and $100\Gamma_{\text{BG}}$ (red). The main effect of raising the intensity of the ionising background is to increase the transmission on the blue side of the line. The skewness parameter, S_W , varies non-monotonically for similar reasons as those mentioned above: because of the long blue tail in the spectrum, S_W is very negative for the case of $10\Gamma_{\text{BG}}$, while the spectrum becomes almost symmetric

² Here, we denote the flux density in pixel number 'i' as $f(x_i)$. The parameter S_W , which has units of \AA , is defined as $S_W \equiv [\lambda_{10,\text{red}} - \lambda_{10,\text{blue}}]S$, where $\lambda_{10,\text{red/blue}}$ are the observed wavelengths at which the flux drops to 10% of its peak value, and $S = \frac{1}{I\sigma^3} \sum_{i=1}^n (x_i - \bar{x})^3 f(x_i)$, where $I = \sum f(x_i)$, $\bar{x} = \sum x_i f(x_i)/I$ and $\sigma = [\sum (x_i - \bar{x})^2 f(x_i)/I]^{1/2}$. For a detailed definition and discussion of the skewness parameter, the reader is referred to the Appendix of Kashikawa et al. (2006).

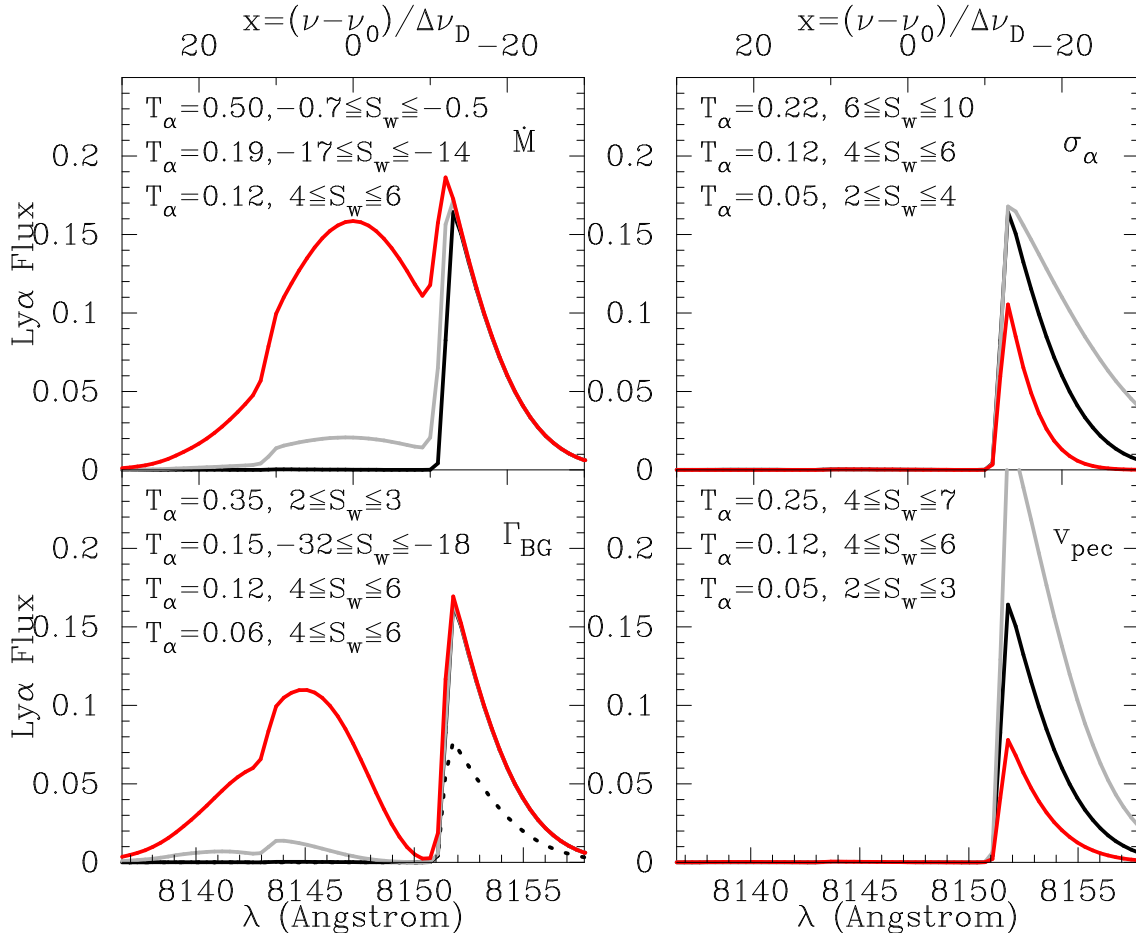


Figure 4. The observed Ly α line from $z = 5.7$ galaxies in a reionised IGM for a range of different models. The upper right corner of each panel shows the model-parameter that is varied. *Top Left:* $\dot{M}_* = 10M_\odot/\text{yr}$ (black), $\dot{M}_* = 10^2M_\odot/\text{yr}$ (grey) and $\dot{M}_* = 10^3M_\odot/\text{yr}$ (red). *Top Right:* $\sigma_\alpha = 1.0v_{\text{circ}}$ (black), $\sigma_\alpha = 0.7v_{\text{circ}}$ (red) and $\sigma_\alpha = 1.5v_{\text{circ}}$ (grey). *Lower Left:* Variation of the ionising background: no ionising background (dotted), Γ_{BG} (black), $10\Gamma_{\text{BG}}$ (grey) and $100\Gamma_{\text{BG}}$ (red). *Lower Right:* Impact of galaxies peculiar velocity: $v_{\text{pec}} = 0$ (black), $v_{\text{pec}} = -0.5\sigma_\alpha$ (red) and $v_{\text{pec}} = 0.5\sigma_\alpha$ (grey). For each model the total transmission, T_α and the skewness of the line, S_W , are shown.

again for the case of $100\Gamma_{\text{BG}}$. The total IGM transmission depends only weakly on the intensity of the ionising background. The reason is that the transmission is determined strongly by the neutral fraction in the infalling gas, which is set primarily by the strength of the ionising luminosity of the galaxy. This can be understood as follows: define the ‘proximity radius’, r_{prox} , as the radius at which the photoionisation rate due to the galaxies ionising photons equals that of the ionising background ($\Gamma_{\text{BG}} = \Gamma_{\text{Gal}}$). For the fiducial model, the proximity radius lies at $r_{\text{prox}} \sim 200$ kpc ($\sim 10r_{\text{vir}}$), which is well outside the infall region. For $r \ll r_{\text{prox}}$, the ionisation rate due to ionising background makes up only $\sim (r/r_{\text{prox}})^2 \sim [0.01 - 0.25]$ of the total ionisation rate within the infall region [in which $r \sim (1 \rightarrow 5)r_{\text{vir}}$, see § 3.1]. As a result, raising Γ_{BG} by a factor of ~ 10 only contributes significantly to Γ_{tot} in the outer layers of the infall region.

Also shown is the spectrum that would be observed when the ionising background is absent, $\Gamma_{\text{BG}} = 0.0$ (*dotted line*). The damping wing of the neutral IGM (outside of the HII sphere created by this galaxy), significantly reduces the flux redward of the infall feature as well. This damping wing

optical depth is only important when the neutral fraction in the IGM is large $x_{\text{HI}} \gtrsim 0.1$ (Santos 2004)³

- *Lower Right:* Impact of galaxy peculiar velocity: $v_{\text{pec}} = 0 \text{ km s}^{-1}$ (black), $v_{\text{pec}} = -0.5\sigma_\alpha$ (red) and $v_{\text{pec}} = 0.5\sigma_\alpha$ (grey). A negative peculiar velocity corresponds to the galaxy receding from the IGM. Clearly, more flux is transmitted towards larger negative velocities. The choice $v_{\text{pec}} = -v_{\text{circ}}$ is equivalent to models that use a static IGM, and would result in $T_\alpha \sim 0.5$. Furthermore, the shape of the Ly α line is quite insensitive to v_{pec} : all lines are asymmetric with a sharp cut-off on the blue side of the line.

Lastly, we investigate is the impact of the radial dependent enhancement of the ionising background due to clustered sources. We showed in § 3.3 that this enhancement, denoted by $B_c(r)$, can be as large as 10^2 , particularly in the close

³ The size of the Stromgren sphere was calculated from $\dot{Q}_H \times t_{\text{gal}} = \int_{r_{\text{vir}}}^{R_s} 4\pi r^2 n_H(r) dr$, in which $t_{\text{gal}} = 3 \times 10^8 \text{ yr}$, is the life time of the galaxy. The neutral fraction in the IGM for $r > R_s$ as set to 1, while for $r < R_s$ photoionisation equilibrium was assumed (Eq 6).

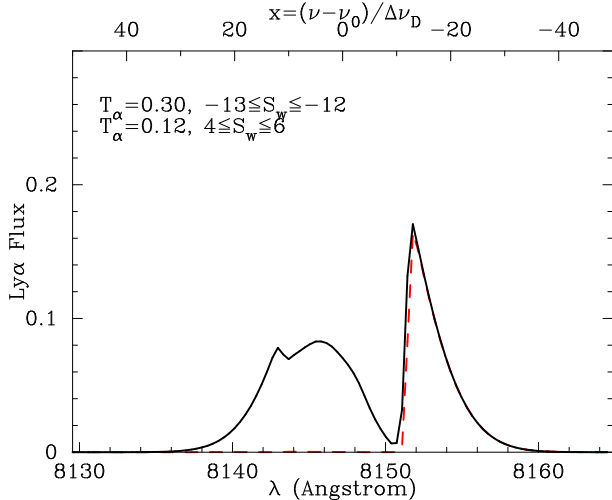


Figure 5. The impact of an enhanced ionising background due to clustered sources surrounding a galaxy on its observed Ly α line. The *red dashed line* is the fiducial case with $B_c(r) = 1$, whereas the *black solid line* shows the case in which $B_c(r)$ takes the form shown in Fig. 2 (the case of $\lambda = 1$ Mpc). The blue side of the line is significantly enhanced, resulting in an increased transmission, $T_\alpha = 0.30$. Note that because of the skewness of $-13\text{\AA} \leq S_w \leq -12\text{\AA}$, this LAE would have been misidentified as a low redshift interloper (if the Ly α line were its only observed feature, see § 5.4).

vicinity of the galaxy. In Figure 5 we show the observed Ly α line for the profile $B_c(r)$ presented in the top panel of Fig. 2 (*black solid line*, $\lambda = 1$ Mpc). The *red dashed line* represents the fiducial case with $B_c(r) = 1$ for comparison. The figure shows that the blue side of the line is significantly enhanced (as we noticed above, see the lower left panel of Fig 4), resulting in a more prominent 'dip' in the spectrum. The overall transmission is enhanced by almost a factor of 3 to $T_\alpha = 0.30$. The skewness of the line is $-13\text{\AA} \leq S_w \leq -12\text{\AA}$, and therefore, this line would not be identified as a high-redshift LAE (see § 5.4 for further discussion). It is interesting to note that since λ decreases with redshift, the boost in the ionising background increases with redshift, which in turn implies that more Ly α lines may have $S_w \lesssim 3\text{\AA}$ towards higher redshift.

We have found the observed shape of the Ly α line to vary widely, depending on \dot{M}_* , Γ_{BG} , σ_α and the systemic velocity of the line, v_{pec} . The main results can be summarised as follows:

(i) For large star formation rates and strong boosts of the ionising background by clustering of nearby sources, the Ly α line loses its trademark asymmetry (the skewness parameter for these models is $S_w \lesssim 3\text{\AA}$). This may become more common towards higher redshift. Taniguchi et al. (2005); Kashikawa et al. (2006) found 20–30% of their LAE-candidates to have symmetric lines. It could be that at least some of these are LAEs, as opposed to [O II] $\lambda 3727$ emitters. This is discussed in more detail in § 5.4.

(ii) For most models, however, the Ly α line is asymmetric with a sharp cut-off on the blue side, and skewness parameters of $S_w \gtrsim 3\text{\AA}$. In such cases, the IGM scatters more than half of the Ly α flux out of our line of sight, with mean transmissions of typically $T_\alpha = 0.1 – 0.3$. Further-

more, infall causes the peak of the Ly α line to be redshifted relative to the true line center.

(iii) The Full Width at Half Maximum (FWHM) of the line is $\lesssim v_{\text{circ}}$ for most models, apart from those with large \dot{M}_* , v_{pec} , σ_α or $B_c(r)$. Models with large \dot{M}_* and/or $B_c(r)$ have $S_w \lesssim 3\text{\AA}$, and so produce either broad symmetric lines or lines that are asymmetric with skewness parameters that are negative.

4.2 The Mean IGM Ly α Transmission Around Galaxies

The previous discussion focused on the change in the Ly α line shape and Ly α transmission as a function of star-formation rate, ionising background, the width of the intrinsic Ly α and the peculiar velocity v_{pec} . These calculations focused on $z = 5.7$ galaxies. Here, we investigate the total transmitted flux for the fiducial model in an ionised IGM (i.e. $f_{\text{esc}} = 0.1$, $v_{\text{pec}} = 0$, $\sigma_\alpha = v_{\text{circ}}$ and $Z = 0.05$) at additional redshifts of $z = 4.5$ and $z = 6.5$ as a function of \dot{M}_* . Thus we have assumed that reionisation was completed by $z = 6.5$, although evidence exists from high redshift quasars may suggest otherwise (Wyithe & Loeb 2004; Mesinger & Haiman 2004, 2006). However, the analysis presented here also applies when galaxies at $z = 6.5$ are embedded in large HII bubbles which are expected to exist prior to the end of reionisation (see § 5.5 for a more detailed discussion). The impact of varying the other model parameters can be inferred from Figure 4.

The results of this calculation are shown in the lower panel of Figure 6. The *black*, *red* and *grey* lines represent galaxies at $z = 4.5$, $z = 5.7$ and $z = 6.5$, respectively. The *grey dotted line* represents the scenario in which the ionising background is set to 0 at $z = 6.5$. The damping wing of hydrogen in the neutral IGM strongly suppresses the transmission as (we noticed already in § 4.1). At all redshifts, $T_\alpha \sim 0.1$ for $\dot{M}_* \lesssim 10M_\odot/\text{yr}$. For larger star formation rates, the mean transmission increases slowly and reaches the value $T_\alpha = 0.3$ only when $\dot{M}_* \sim 90M_\odot/\text{yr}$, $\dot{M}_* \sim 300M_\odot/\text{yr}$ and $\dot{M}_* \sim 500M_\odot/\text{yr}$ at $z = 4.5$, $z = 5.7$ and $z = 6.5$, respectively. Figure 6 strongly suggests that not properly accounting for scattering in the IGM, can lead to significant underestimates of $L_{\text{Ly}\alpha}$, and thus of the star formation rates. In the upper panel, we show the observable Ly α flux as a function of star formation rate. The *solid/dashed lines* represent calculations in which the transmission was/was-not accounted for. The thin *horizontal lines* denote the detection thresholds of recently performed Ly α surveys at $z = 4.5$ (Dawson et al. 2004), $z = 5.7$ (Shimasaku et al. 2006) and $z = 6.5$ (Taniguchi et al. 2005). As an example, for a given Ly α flux from a $z = 5.7$ galaxy, say $S_\alpha = 10^{-17} \text{ erg s}^{-1} \text{ cm}^{-2}$, ignoring the IGM would lead to an estimated star formation rate of $\dot{M}_* = 2M_\odot/\text{yr}$, while the actual star formation rate was $\dot{M}_* \sim 20M_\odot/\text{yr}$. Therefore, not accounting for IGM scattering could lead to substantial underestimates of the Ly α -derived star formation rates occurring in LAEs. We discuss this in more detail in § 5.1.

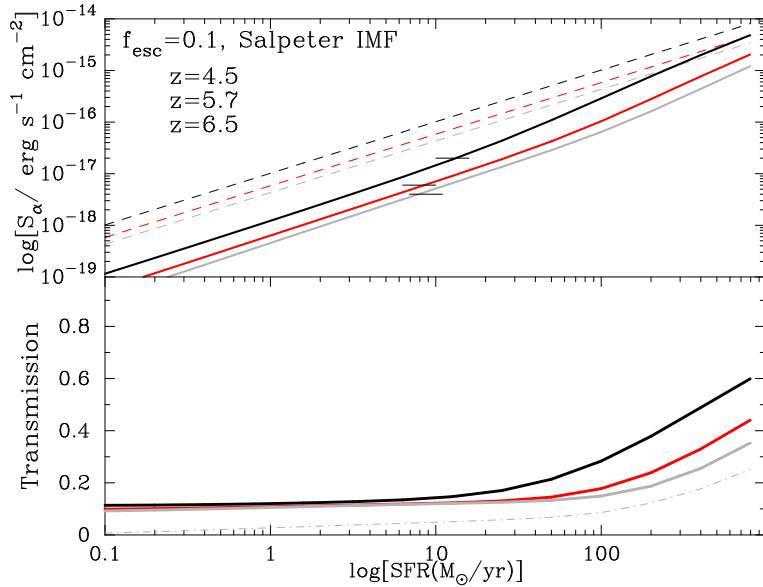


Figure 6. *Bottom Panel:* Mean IGM transmission for a galaxy in a halo of mass $M_{\text{tot}} = 10^{11} M_{\odot}$ as a function of the star formation rate (\dot{M}_*), at $z = 4.5$ (black), $z = 5.7$ (red) and $z = 6.5$ (grey). The dotted grey line represents the scenario in which the IGM is completely neutral at $z = 6.5$. *Top Panel:* The observed Ly α flux for our fiducial model as a function of \dot{M}_* , at the same redshifts presented in the *bottom panel*. The solid lines and dashed lines show the observed flux when the IGM transmission is/is not accounted for respectively. For all SFRs the mean transmission is significantly less than 1, which may lead to an underestimate of \dot{M}_* . The thin horizontal lines denote the detection thresholds of recently performed Ly α surveys at $z = 4.5$, $z = 5.7$ and $z = 6.5$ (see text).

4.3 Ly α Transmission in the Absence of a Virial Shock

Our model assumes that no absorption takes place inside the virial radius. The motivation for this assumption is that the virial temperature is well above 10^4 K for the halos considered in this paper, and as a result, the virialised gas is collisionally ionised to a very high level (in our models the collisional ionisation rate of hydrogen in the virialised gas is $\sim 10^{-10} \text{ s}^{-1}$). However, the cooling time of this gas is short. In particular, the cooling time is shorter than the dynamical time of the system (Haiman et al. 2000), and hence the gas rapidly loses its pressure support and collapses further. Indeed, it has been argued that because of this efficient cooling, the virial shock does not exist in halos with masses below $M \lesssim 2 \times 10^{11} M_{\odot}$ (the precise mass depends on the metallicity of the gas, Birnboim & Dekel, 2003). We may therefore expect that infall continues at radii less than the virial radius. The precise infall velocity profile of this gas is not well known. However, the absence of a virial shock would reduce the Ly α transmission further, especially in cases where the infall within the virial radius occurs at speeds exceeding v_{circ} , because then, the absorption would extend even further into the red part of the line.

5 DISCUSSION

5.1 Deriving Star formation Rates from Ly α Fluxes

In § 4.2 we have shown how Ly α scattering in the IGM can reduce the detected Ly α flux by up to an order of magnitude. This implies that estimates of the star formation rate based on Ly α fluxes generally underestimate the true star

formation rate. Shimasaku et al. (2006) found 28 spectroscopically confirmed LAEs. They found that the Ly α derived star-formation density for their survey volume lies a factor of ~ 3 below the estimates of Bouwens et al. (2006, down to the same UV-luminosity). Recently, Taniguchi et al. (2005) found that the Ly α derived star formation rates lie, on average, a factor of ~ 5 below values derived from the UV-continuum measurements. The typical UV-derived star formation rates for galaxies in their sample were in the range $\sim 5 - 45 M_{\odot}/\text{yr}$, which according to our Figure 6 would translate to $T_{\alpha} \sim 0.1 - 0.2$. Scattering in the IGM therefore fully accounts for the apparent discrepancy between UV and Ly α derived star formation rates.

Note however, that the discrepancy between UV and Ly α derived star formation rates, is not considered a serious issue. The reason for this is that Ly α photons may be subject to a different amount of dust attenuation than UV-continuum photons. For example, scattering of Ly α photons through the ISM increases their total traversed path through the galaxy, making Ly α photons more vulnerable to dust attenuation (on the other hand, in the case of a multiphase ISM, the Ly α may be subject to less attenuation, see § 2.3). Therefore, the observed discrepancy between Ly α and UV-derived star formation rates can also be interpreted as resulting from Ly α being preferentially destroyed by dust inside the galaxy (see Kunth et al. 1998, for a discussion on the difficulties associated with estimating star formation rates from Ly α fluxes). However, it is interesting that our low value of the transmission through an ionised IGM provides a natural explanation for the discrepancy.

5.2 Constraints from the Observed Ly α Line Width+EW.

Figures 3-5 show that the typical observed line width of our model LAEs is $\sim 2 - 10$ Å, with the fiducial model having a FWHM of ~ 3 Å. The bulk of the observed LAEs in Shimasaku et al. (2006) have a FWHM in the range $\sim 2 - 14$ Å, with the majority of the LAEs having FWHM $\gtrsim 5$ Å. These values of the FWHM can be explained with larger v_{pec} or σ_{α} . A larger star formation rate, or a boost in the ionising background have the same effect, but probably not while maintaining $S_w \gtrsim 3$ Å. In particular, the high end of the range of observed FWHM cannot be explained this way. An elegant explanation for the large line width systems is provided by back-scattering off a superwind driven shell of neutral gas (Ahn et al. 2003; Ahn 2004). Here, Ly α emitted by the galaxy scatters off an thick neutral shell that is receding from the galaxy with a velocity v_{exp} . Photons that are scattered back to the galaxy have now picked up a redshift of $2v_{\text{exp}}$, and may make it through the shell without being scattered. Ahn et al. (2003) have shown that the Ly α line can easily be broadened by several times v_{exp} . This back-scattered Ly α would all be on the red-side of the line center, and would thus be transmitted through the IGM.

Kashikawa et al. (2006) have found that marginal evidence exists for an anti-correlation between the Ly α FWHM and the derived Ly α luminosity, i.e. the measured Ly α flux. This is contrary to what one would expect for the superwind scenario sketched above (in which the IGM transmission is larger) unless the wind-driven shells contain dust which could reduce the escape fraction of Ly α photons from the galaxy. An alternative explanation for this observation may be that that the broadest lines are broadened by resonant scattering (although we find this more unlikely as discussed in § 2.2).

5.3 Comparing the Ly α and LGB Luminosity Functions.

Kashikawa et al. (2006) compared the restframe-UV luminosity function of their $z = 6.5$ LAE sample with that of the i-drop-out sample of Bouwens et al. (2006) and found that the faint end slope for LAEs at $z = 5.7$ (Hu et al. 2004; Shimasaku et al. 2006) and $z = 6.5$ (Kashikawa et al. 2006) is flatter than that of the i-drop out galaxies. The differences between the LAE and i-drop out UV-luminosity functions only becomes prominent for $M_{\text{UV}} \gtrsim -20.5$. Kashikawa et al. (2006) suggest that this is most likely due to a combination of detection incompleteness at faint Ly α and UV-fluxes ($M_{\text{UV}} \gtrsim -20.3$ corresponds to the $3 - \sigma$ detection threshold). Using the standard conversion from UV-continuum flux density to star formation rate (e.g. Kennicutt 1998), we find that $M_{\text{UV}} \gtrsim -20.5$ corresponds to $\dot{M}_* \lesssim 8.0 M_{\odot} \text{ yr}^{-1}$. According to Figure 6, the IGM transmission associated with these star formation rates is low, $\mathcal{T}_{\alpha} \lesssim 0.12$ in this case, and the expected Ly α flux is $S_{\alpha} \lesssim 6 \times 10^{-18} \text{ erg s}^{-1} \text{ cm}^{-2}$; almost exactly the detection threshold. For lower star formation rates (and higher M_{UV}) a detection in Ly α requires a larger IGM transmission around these galaxies, which requires a large v_{pec} , or σ_{α} (§ 4.1). This suggests that at fainter Ly α (and UV) fluxes indeed only a small subset of LAEs is currently detected.

5.4 Symmetric and Double Peaked Ly α Emission Lines; A Source of Selection Bias?

In § 4.1 we found that the Ly α line becomes either symmetric or asymmetric in the wrong direction ($S_w \lesssim 3$ Å) for large star formation rates and for strong enhancements of the ionising background. This suggests that the current criterion of asymmetry introduces biases against detection of galaxies undergoing intense episodes of star formation and/or embedded in regions of enhanced ionising background. In practice however, the criterion $S_w > 3$ Å is used in combination with the broad band photometry in the B and V-bands (e.g. Shimasaku et al. 2006). High-redshift LAEs are practically invisible in both these bands due to absorption in the IGM blueward of the rest-frame Ly α frequency. Therefore, only those objects having both $S_w < 3$ Å and a detection in the B or V Band are classified as low redshift interlopers. Objects for which $S_w < 3$ Å that are not detected in B and V are classified as an "unclear" objects. Approximately 15% of the objects detected by Shimasaku et al. (2006) and Kashikawa et al. (2006) were classified as such and could thus be high-redshift LAEs. Six out of 34 of the $S_w > 3$ Å objects from Shimasaku et al. (2006) are bright in B or V. Shimasaku et al. (2006) argue that these objects are genuine LAEs, with the B/V flux contributed by nearby faint, contaminating sources. Likewise, some of the 19 objects in their 63-object spectroscopic sample with symmetric lines and detection in B/V could be LAEs and foreground B/V sources. However, the above considerations suggest a small fraction of $S_w < 3$ Å LAEs and argue against a serious selection bias.

The low number of high-redshift LAEs with $S_w \lesssim 3$ Å could be attributed to a small number of LAEs being embedded in regions of strongly enhanced ionising backgrounds, or to a small number of galaxies undergoing intense episodes of star formation. It could also imply that the IGM surrounding LAEs is denser than we have assumed. To make observed Ly α lines have $S_w > 3$ Å, one needs to enhance the absorption in the IGM. Conversely, if we ignore infall, or lower the IGM density, then lower star formation rates or smaller enhancements of the ionising background are required to produce $S_w \lesssim 3$ Å-lines. We point out that although high-redshift LAEs with symmetric lines appear to be rare, these objects may be cosmologically very interesting. For example, recent simulations by Li et al. (2006) show that the star formation rates in progenitor galaxies of the luminous $z = 6$ quasars may be as large as $\dot{M}_* = 10^4 M_{\odot} \text{ yr}^{-1}$ (at $z = 6 - 14$). These galaxies would almost certainly have $S_w \lesssim 3$ Å Ly α lines.

Some Ly α emission lines shown in Figures 6 and 5 with $S_w \lesssim 3$ Å have two peaks that are separated by ~ 7 Å. Coincidentally, this is almost exactly the separation expected for a resolved [OII] doublet (~ 6.6 Å, in the observed frame at $z = 1.2$). In cases where neither B nor V is detected, such a Ly α emitter may be confused with a $z = 1.2$ [O II] doublet. Whether or not a Ly α line consists of two peaks depends on the following considerations. The largest contribution to the Ly α opacity at a frequency x comes from the resonant region (defined as the region where the photons are at resonance, Eq 8). Therefore, if the resonant region lies a distance r from the central galaxies, the total opacity to photons at frequency x can be approx-

imated by $\tau(x) \sim n_H(r)x_H(r)v_{\text{th}}/[dv/dr] \propto n_H^2(r)/J(r)$. Here, we used the relation $x_H(r) \propto n_H(r)/J(r)$, and assumed for simplicity that the variation of dv/dr with radius can be ignored. In our model, photons just blueward of the observed (red) peak, resonate with gas near the virial radius that falls inward at the maximum speed. If $n_H(r)$ decreases faster than $[J(r)]^{1/2}$ with increasing r , then the opacity decreases towards bluer wavelengths and produces a 'dip' in the observed spectrum. In our models $n_H(r) \propto r^{-1}$, while to produce a dip requires $J(r)$ to change more slowly than r^{-2} , which is indeed the case when the ionising background is enhanced (Fig 2). The precise location of the dip, and thus the separation of the two peaks, depends on the exact radial dependence of the density and velocity profiles of the surrounding gas, in addition to the ionising radiation field. Note that double peaked, spatially extended, Ly α emission has been observed (e.g. van Ojik et al. 1997; Wilman et al. 2005), often around radio galaxies. Various other mechanisms including superwinds and resonant scattering can create double peaked Ly α emission lines (see Verhamme et al. 2006, for a more detailed discussion on this issue).

5.5 Ly α Transmission at Higher Redshifts: $z \geq 7$

Our analysis has focused on the redshifts bins $z = 4.5, 5.7$ and $z = 6.5$, corresponding to windows of reduced atmospheric OH emission. Other windows exist at $z \sim 7$, $z = 8$ and $z = 8.8$ (Nilsson et al. 2006). Ly α emission from higher redshifts is expected to be detected soon (see Iye et al. 2006, for a detection of a $z = 7.0$ galaxy). Our analysis is expected to be applicable here as well, even if reionisation was not completed until $z = 6 - 6.5$. The reason is that prior to overlap, large bubbles (with typical sizes of $\sim 1 - 10$ physical Mpc, hereafter pMpc) of ionised gas are expected to populate the IGM, each of which may harbor many Ly α emitting galaxies (Furlanetto et al. 2004a,b; Wyithe & Loeb 2005).

The analysis presented by Santos (2004) in which a galaxy sits inside its own HII region embedded in a neutral IGM, does not apply to most galaxies in this scenario. In particular, absorption by the damping wing of neutral intergalactic hydrogen is less important for galaxies inside these large HII regions. This is illustrated in Figure 7. Here, we show the Ly α emission line of a galaxy at $z = 8$ (the other model parameters, except for Γ_{BG} , correspond to the fiducial model which is described in § 4) for the case in which the galaxy is surrounded by its own HII region (which is ~ 0.7 pMpc for our model), and for cases in which the galaxy is embedded within a larger HII region created by an ensemble of nearby sources. The IGM outside the bubble is assumed to be neutral. The other cases shown are for $R_{\text{HII}} = 2.0$ pMpc (red line) and $R_{\text{HII}} = 10.0$ pMpc (grey line).⁴

Figure 7 shows that damping wing absorption on the red side of the Ly α line center becomes decreasingly important towards larger R_{HII} . However, resonant absorption the

⁴ We have assumed that the IGM is completely neutral outside the HII bubbles. Partial ionisation of the surrounding IGM (e.g. by X-Rays, Oh 2001; Venkatesan et al. 2001), and neighboring bubbles reduce the contribution of the damping wing to the IGM transmission, in which case the dependence of the IGM transmission on HII bubble size is even smaller.

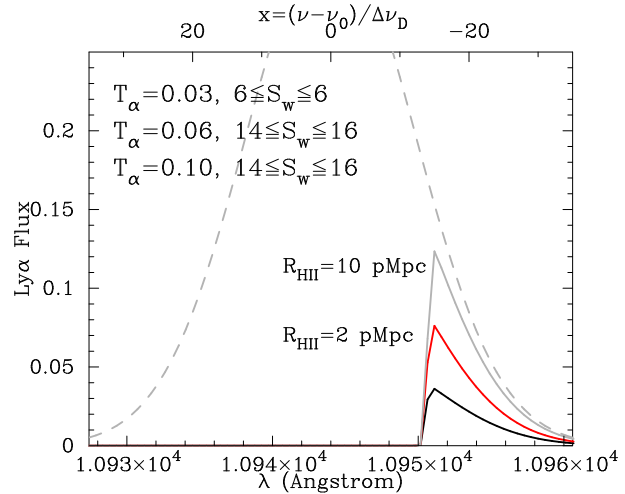


Figure 7. The observed Ly α line of a $z = 8.0$ galaxy (fiducial model parameters) for the case in which the galaxy carves its own HII region out of a fully neutral IGM (black line); when this galaxy lies in the center of a larger HII bubble of 2.0 pMpc (red line); and 10.0 pMpc (grey line). For each model T_{α} and S_W , are shown. The presence of large 'über-HII region' boosts the Ly α transmission on the red side of the line. The *dashed grey line* represents the intrinsic spectrum.

in infall region erases the Ly α line for $\lambda \lesssim 1.095 \times 10^4$ Å in all cases. Since the transmission is regulated primarily by resonant absorption in the infall region and by damping wing absorption in the neutral IGM, T_{α} is practically insensitive to the neutral fraction of hydrogen inside the bubble at $r \gtrsim 3 - 5r_{\text{vir}}$. The overall transmission for the three cases is $T_{\alpha} = 0.03$ ($R_{\text{HII}} = 0.7$ pMpc), $T_{\alpha} = 0.06$ ($R_{\text{HII}} = 2.0$ pMpc) and $T_{\alpha} = 0.10$ ($R_{\text{HII}} = 10.0$ pMpc). Therefore, at first glance, the presence of large HII bubbles prior to overlap boosts the Ly α transmission by only a factor of ~ 3 . We obtained similar results for a halo mass of $M_{\text{tot}} = 10^{10} M_{\odot}$, for cases in which the Ly α line is intrinsically narrower/broader ($\sigma_{\alpha} = 0.7/1.5v_{\text{circ}}$), and for cases in which the galaxy possesses a peculiar velocity with respect to the surrounding IGM ($v_{\text{pec}} = \pm 0.5v_{\text{circ}}$). However, we caution that when calculating the Stromgren radius, we (incorrectly) ignored recombinations in the HII region. Therefore, the Stromgren radius we calculate for our model is actually too large (although note that ionising radiation produced by a cluster of fainter, undetected, sources surrounding the galaxy may increase the Stromgren radius, e.g. Wyithe & Loeb, 2005). If we decrease the Stromgren radius by a factor of ~ 3 , then T_{α} decreases by an additional factor of almost 2. Furthermore, for galaxies in large bubbles the transmission could be boosted significantly due to nearby clustered sources (but note that this would likely result in Ly α lines with $S_W < 3$ Å, see § 3.3).

The average HII-bubble size is related to the globally averaged neutral fraction of the universe by volume, $x_{\text{i},\text{v}}$ (Furlanetto et al. 2006), and therefore it is useful to calculate the IGM transmission as a function of HII-bubble size for various models. The result of this calculation is shown in Figure 8, where we considered cases at $z = 6.5$ (dotted lines) and $z = 8.0$ (solid lines) for $\dot{M}_* = 10 M_{\odot} \text{ yr}^{-1}$ and $\dot{M}_* = 10^2 M_{\odot} \text{ yr}^{-1}$. The minimum radius for each line corresponds to cases of isolated galaxies in an otherwise neu-

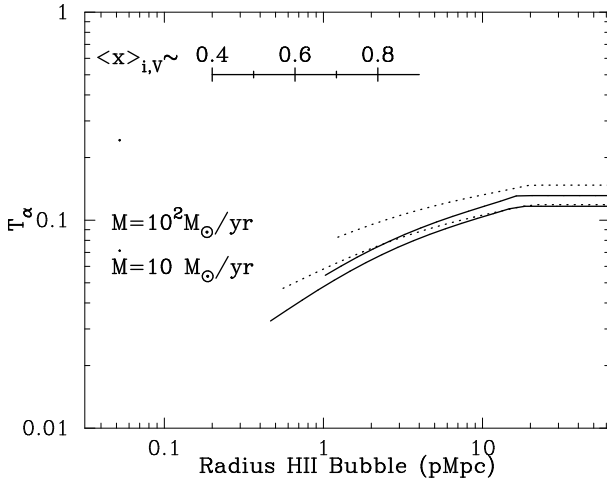


Figure 8. The fraction of Ly α that is transmitted through the IGM as a function of HII-bubble size prior to the completion of reionisation. We have shown cases at $z = 6.5$ (dotted lines) and $z = 8.0$ (solid lines) for $\dot{M}_* = 10 M_\odot/\text{yr}$ and $\dot{M}_* = 10^2 M_\odot/\text{yr}$. The minimum radius for each line corresponds to cases of isolated galaxies in an otherwise neutral IGM. The globally averaged neutral fraction of the universe by volume, $x_{i,v}$, is related to the characteristic HII-bubble size (Furlanetto et al. 2006). An approximate relation between R_{HII} and $x_{i,v}$ is also shown.

tral IGM. The relation between HII bubble size and neutral fraction depends on the nature of the ionising sources, the abundance of Lyman-limit systems, and on the redshift (Furlanetto et al. 2006; McQuinn et al. 2006). An approximate relation between the characteristic HII bubble size R_{HII} and $x_{i,v}$ derived by Furlanetto et al. (2006) is shown in the Figure for $0.4 < x_{i,v} < 0.9$. The figure shows that the transmission drops only by a factor of ~ 3 compared to cases in which the IGM is fully reionised. As was mentioned above, part of the reason for this low contrast is that by ignoring recombinations within the Stromgren-sphere, we may have overestimated its size. Furthermore, clustered sources inside the large über-HII bubbles could significantly boost the local ionising background, which would increase the transmission (see § 3.3).

This result has the following implication: as reionisation of the IGM proceeds, HII bubbles grow larger in time until they overlap. The transmission of Ly α photons emitted by a galaxy inside such an HII bubble continuously grows with bubble size (Furlanetto et al. 2006). The precise dependence of T_α on HII bubble size depends on the strength of the ionising background inside the bubbles. At overlap a ‘jump’ in the ionising background may occur (Gnedin 2000, although see Furlanetto & Oh, 2005). If such a jump occurs it will not result in a jump in the IGM transmission around LAEs, as we showed in § 4.1. Therefore, LAEs of comparable luminosity should not appear to be significantly dimmer prior to overlap. The evolution in the Ly α luminosity function between $z = 5.7$ and $z = 6.5$ found by Kashikawa et al. (2006) is therefore not necessarily due to reionisation (unless the characteristic bubble size evolved very rapidly between $z = 5.7$ and $z = 6.5$, see Dijkstra et al. 2007 for a more detailed discussion).

6 CONCLUSIONS

We have calculated the impact of an ionised intergalactic medium on the Ly α line emitted by galaxies at $z \geq 4.5$. Our model accounts for gas clumping in the IGM and for the fact that high-redshift galaxies typically reside in overdense regions, which causes the velocity field of the IGM to deviate from the Hubble flow. We calculated the observed shape of the Ly α line as a function of the galaxies ionising luminosity, the intrinsic width and systemic velocity of the Ly α line and the extra-galactic UV-background (which may be enhanced due to unseen clustered sources by a factor of ~ 100).

We found that the observed shape of the Ly α line can display a wide range of shapes, depending on the precise values of \dot{M}_* , Γ_{BG} , σ_α and v_{pec} (see § 4.1 and Fig 4). Our most important findings are:

- For large star formation rates, the strong asymmetry of the Ly α line (believed to be the defining characteristic of a high-redshift Ly α line) vanishes. For example, given $M_{\text{tot}} = 10^{11} M_\odot$ ($M_\odot = 10^{10} M_\odot$), a star formation rate of $\dot{M}_* = 100 M_\odot \text{ yr}^{-1}$ ($\dot{M}_* = 10 M_\odot \text{ yr}^{-1}$) produces $S_w < 0$, whereas the value $S_w \geq 3 \text{ \AA}$ has been shown to distinguish between confirmed high-redshift LAEs and lower redshift interlopers. Also, we find that $S_w \lesssim 3 \text{ \AA}$ for galaxies in which the ionising background was boosted significantly (which may become more common towards higher redshift) by surrounding clustered galaxies. An enhanced ionising background may occasionally result in a double-peaked Ly α emission line, mimicking a lower redshift [OII] emission line. The criterion $S_w \geq 3 \text{ \AA}$ could therefore introduce a selection bias against galaxies with high star formation rates and/or galaxies embedded in an enhanced extragalactic UV-background. However, at $z=5.7$ and $z=6.5$ this is not a serious issue as only $\sim 15\%$ of the known Ly α emitter candidates has $S_w \lesssim 3 \text{ \AA}$. Nevertheless, recent cosmological simulations have shown that star formation rates as large as $\dot{M}_* = 10^4 M_\odot \text{ yr}^{-1}$ may occur at $z = 6 - 14$ (Li et al. 2006). These galaxies, while rare, would almost certainly have symmetric Ly α lines.

• In most models, the Ly α line is asymmetric ($S_w > 3 \text{ \AA}$) with a sharp cut-off on the blue side. In these models, the IGM typically scatters more than half of the Ly α flux out of the line of sight, with a mean transmission of $T_\alpha = 0.1 - 0.3$.

• The low values of the IGM transmission found in this paper suggest that not accounting for IGM scattering could lead to substantial underestimates of the Ly α -derived star formation rates in LAEs. Although both the UV and Ly α -derived star formation rates are subject to large uncertainties, our model naturally explains the apparent discrepancy that currently exists in the literature between the two.

• Clustering of sources prior to overlap boosts the detectability of LAEs, as ensembles of clustered sources produce large HII bubbles. This reduces the impact the damping wing of the neutral IGM (Furlanetto et al. 2006). The precise dependence of T_α on HII bubble size depends on the strength of the ionising background inside the bubbles. Furthermore, the possible boost in the ionising background that follows the overlap of HII bubbles (when reionisation is completed) barely increases the IGM transmission. Increasing the local ionising background by a factor of ~ 10 only increases the IGM transmission by a few per cent. This sug-

gests that LAEs of comparable luminosity should not appear to be significantly dimmer prior to overlap.

- The observed physical width of the Ly α line contains useful information. In particular, Our models have difficulties reproducing observed FWHM $\gtrsim 10$ Å, while conserving the asymmetry of the line, and we conclude that these LAEs are most likely to be galaxies with a superwind-driven outflow.

Our result that LAEs are not expected to become significantly brighter in a post-overlap IGM, naively implies that LAEs do not provide a direct probe of the end of reionisation. However, our work suggests that LAEs are not expected to dim significantly faster than $\propto d_L^{-2}(z)$ at $z \gtrsim 7$. We therefore expect Ly α surveys to be very fruitful in uncovering young galaxies at these higher redshifts, which will allow studies of star formation in the very first galaxies. Constraints on reionisation can then be obtained through various methods which include for example, cross-correlating the distribution of LAEs with intergalactic 21-cm emission (Wyithe & Loeb 2006); or by adding up the ionised volume surrounding individual LAEs as in Malhotra & Rhoads (2006). Moreover, with a large enough sample of LAEs at various redshift bins, it is possible to detect a weak evolution of the IGM transmission, which is expected to exist in our model due to the gradual growth of HII bubbles (Furlanetto et al. 2006; McQuinn et al. 2006; Dijkstra et al. 2007). The constraints on the IGM transmission can be further improved when Ly α luminosity functions are combined with the Ly α emitters' rest-frame UV luminosity functions (as in Kashikawa et al. 2006, also see Dijkstra et al. 2006c). Additionally, since the abundance of observable emitters is modulated by the presence/absence of large HII bubbles, the two-point correlation function of LAEs may be used to constrain the dependence of \mathcal{T}_α on HII-bubble size (Furlanetto et al. 2006; McQuinn et al. 2006), which puts constraints on the strength of the ionising background inside the bubbles.

Finally, we point out that our focus has been on the mean Ly α profile. In reality, fluctuations in the transmission from source to source are likely to exist. For example, the transmission is higher for sources viewed along a particularly low density path. It is highly unlikely that the majority of known LAEs are observed along such paths, as a high transmission is likely to be accompanied with $S_w \lesssim 3$ Å. In future work we will address this scatter in the Ly α transmission in more detail using cosmological simulations.

Acknowledgments JSBW and MD thank the Australian Research Counsel for support and MD thanks the Center for Astrophysics for their hospitality. We thank Avi Loeb for useful discussions. We thank the anonymous referee for his/her careful reading of this manuscript and for a very helpful report that improved the content of this paper.

REFERENCES

Ahn, S.-H., Lee, H.-W., & Lee, H. M. 2003, MNRAS, 340, 863

Ahn, S.-H. 2004, ApJL, 601, L25

Barkana, R., & Loeb, A. 2003, *Nature*, 421, 341

Barkana, R. 2004, MNRAS, 347, 59

Birnboim, Y., & Dekel, A. 2003, MNRAS, 345, 349

Bosma, A. 1981, AJ, 86, 1791

Bouwens, R. J., Illingworth, G. D., Blakeslee, J. P., & Franx, M., accepted for ApJ, 2006, astro-ph/0509641

Bromm, V., Kudritzki, R. P., & Loeb, A. 2001, ApJ, 552, 464

Bunker, A. J., Stanway, E. R., Ellis, R. S., McMahon, R. G., & McCarthy, P. J. 2003, MNRAS, 342, L47

Charlot, S., & Fall, S. M. 1993, ApJ, 415, 580

Dawson, S., et al. 2004, ApJ, 617, 707

Dijkstra, M., Haiman, Z., & Spaans, M. 2006a, ApJ, 649, 14

Dijkstra, M., Haiman, Z., & Spaans, M. 2006b, ApJ, 649, 37

Dijkstra, M., Stuart, J., & Wyithe, B. 2006, MNRAS, 372, 1575

Dijkstra, M., Wyithe, J.S.B., & Haiman, Z., 2007, submitted to MNRAS, astroph/0611195

Loeb, A., & Eisenstein, D. J. 1995, ApJ, 448, 17

Fan, X., et al. 2006, AJ, 132, 117

Furlanetto, S. R., Hernquist, L., & Zaldarriaga, M. 2004a, MNRAS, 354, 695

Furlanetto, S. R., Zaldarriaga, M., & Hernquist, L. 2004b, ApJ, 613, 1

Furlanetto, S. R., & Oh, S. P. 2005, MNRAS, 363, 1031

Furlanetto, S. R., Zaldarriaga, M., & Hernquist, L. 2006, MNRAS, 365, 1012

Gnedin, N. Y. 2000, ApJ, 535, 530

Gunn, J. E., & Peterson, B. A. 1965, ApJ, 142, 1633

Haiman, Z., Spaans, M., & Quataert, E. 2000, ApJL, 537, L5

Haiman, Z. 2002, ApJL, 576, L1

Hansen, M., & Oh, S. P. 2006, MNRAS, 367, 979

Harrington, J. P. 1973, MNRAS, 162, 43

Hu, E. M., Cowie, L. L., & McMahon, R. G. 1998, ApJL, 502, L99

Hu, E. M., Cowie, L. L., McMahon, R. G., Capak, P., Iwamuro, F., Kneib, J.-P., Maihara, T., & Motohara, K. 2002, ApJL, 568, L75

Hu, E. M., Cowie, L. L., Capak, P., McMahon, R. G., Hayashino, T., & Komiyama, Y. 2004, AJ, 127, 563

Hui, L., & Gnedin, N. Y. 1997, MNRAS, 292, 27

Hui, L., & Haiman, Z. 2003, ApJ, 596, 9

Inoue, A. K., Iwata, I., & Deharveng, J.-M. 2006, MNRAS, 371, L1

Iye, M., et al. 2006, *Nature*, 443, 186

Kashikawa, N., et al. 2006, ArXiv Astrophysics e-prints, arXiv:astro-ph/0604149

Kennicutt, R. C., Jr. 1998, ARA&A, 36, 189

Kodaira, K., et al. 2003, PASJ, 55, L17

Kunth, D., Mas-Hesse, J. M., Terlevich, E., Terlevich, R., Lequeux, J., & Fall, S. M. 1998, A&A, 334, 11

Le Delliou, M., Lacey, C. G., Baugh, C. M., & Morris, S. L. 2006, MNRAS, 365, 712

Li, Y., et al. 2006, ArXiv Astrophysics e-prints, arXiv:astro-ph/0608190

Loeb, A., Barkana, R., & Hernquist, L. 2005, ApJ, 620, 553

Malhotra, S., & Rhoads, J. E. 2002, ApJL, 565, L71

Malhotra, S., & Rhoads, J. E. 2006, ApJL, 647, L95

McQuinn, M., Lidz, A., Zahn, O., Dutta, S., Hernquist, L., & Zaldarriaga, M. 2006, ArXiv Astrophysics e-prints, arXiv:astro-ph/0610094

Mesinger, A., & Haiman, Z. 2004, ApJL, 611, L69

Mesinger, A., & Haiman, Z. 2006, ArXiv Astrophysics e-prints, arXiv:astro-ph/0610258

Miralda-Escudé, J., Haehnelt, M., & Rees, M. J. 2000, ApJ, 530, 1

Neufeld, D. A. 1990, ApJ, 350, 216

Neufeld, D. A. 1991, ApJL, 370, L85

Nilsson, K. K., Fynbo, J. P. U., Moller, P., & Orsi, A. 2006, ArXiv Astrophysics e-prints, arXiv:astro-ph/0611239

Oh, S. P. 2001, ApJ, 553, 499

van Ojik, R., Roettgering, H. J. A., Miley, G. K., & Hunstead, R. W. 1997, A&A, 317, 358

Osterbrock, D. E. 1989, *Astrophysics of gaseous nebulae and active galactic nuclei*, 1989.

Ouchi, M. 2003, Ph.D. Thesis,

Partridge, R. B., & Peebles, P. J. E. 1967, ApJ, 147, 868

Press, W. H., & Schechter, P. 1974, ApJ, 187, 425

Rhoads, J. E., Malhotra, S., Dey, A., Stern, D., Spinrad, H., & Jannuzzi, B. T. 2000, ApJL, 545, L85

Santos, M. R. 2004, MNRAS, 349, 1137

Schaerer, D. 2003, A&A, 397, 527

Shapley, A. E., Steidel, C. C., Pettini, M., & Adelberger, K. L. 2003, ApJ, 588, 65

Sheth, R. K., & Tormen, G. 1999, MNRAS, 308, 119

Shimasaku, K., et al. 2006, PASJ, 58, 313

Spergel, D. N., et al. 2006, ArXiv Astrophysics e-prints, arXiv:astro-ph/0603449

Stanway, E. R., et al. 2004, ApJL, 604, L13

Stanway, E. R., et al. 2007, ArXiv Astrophysics e-prints, arXiv:astro-ph/0701211

Steidel, C. C., Giavalisco, M., Pettini, M., Dickinson, M., & Adelberger, K. L. 1996, ApJL, 462, L17

Steidel, C. C., Adelberger, K. L., Shapley, A. E., Pettini, M., Dickinson, M., & Giavalisco, M. 2000, ApJ, 532, 170

Taniguchi, Y., et al. 2005, PASJ, 57, 165

Tapken, C., et al. 2006, A&A, 455, 145

Tasitsiomi, A. 2006, ApJ, 645, 792

Trager, S. C., Faber, S. M., Dressler, A., & Oemler, A. J. 1997, ApJ, 485, 92

Tran, K.-V. H., Lilly, S. J., Crampton, D., & Brodwin, M. 2004, ApJL, 612, L89

Venkatesan, A., Giroux, M. L., & Shull, J. M. 2001, ApJ, 563, 1

Verhamme, A., Schaerer, D., & Maselli, A. 2006, ArXiv Astrophysics e-prints, arXiv:astro-ph/0608075

Westra, E., et al. 2006, A&A, 455, 61

Wilman, R. J., Gerssen, J., Bower, R. G., Morris, S. L., Bacon, R., de Zeeuw, P. T., & Davies, R. L. 2005, *Nature*, 436, 227

Wyithe, J. S. B., & Loeb, A. 2004, *Nature*, 432, 194

Wyithe, J. S. B., & Loeb, A. 2004b, *Nature*, 427, 815

Wyithe, J. S. B., & Loeb, A. 2005, ApJ, 625, 1

Wyithe, S., & Loeb, A. 2006, ArXiv Astrophysics e-prints, arXiv:astro-ph/0609734

Zahn, O., Lidz, A., McQuinn, M., Dutta, S., Hernquist, L., Zaldarriaga, M., & Furlanetto, S. R. 2006, ArXiv Astrophysics e-prints, arXiv:astro-ph/0604177

Zheng, Z., & Miralda-Escudé, J. 2002, ApJ, 578, 33

APPENDIX A: THE BOOST IN THE IONISING BACKGROUND DUE TO CLUSTERING OF SOURCES.

We model the ionising background in the overdense regions surrounding massive galaxies using a semi-analytic model for biased galaxy formation near high redshift galaxies. Since we focus on $z > 4$, beyond the peak redshift for quasar activity, we consider the case where AGN do not contribute to the background. Making the assumption that the ionising radiation generated by galaxies was emitted over a Hubble time, and assuming the ionising photon mean-free-path (λ) to be independent of density, we may derive an expression for the ionising background flux at radius R . We first calculate the ionising photon production rate per unit volume from sources surrounding the central galaxies

$$\frac{dN}{dt}(R) = \int_{M_{\min}}^{\infty} dM \left(\frac{4\pi D_*^3 n_{\text{H}}}{3H^{-1}} \right) \frac{dn(R, M_{\text{halo}})}{dM}, \quad (\text{A1})$$

where n_{H} is the hydrogen number density. In this expression the number density of halos surrounding the central halo $dn(R, M_{\text{halo}})/dM$ is found from the Press-Schechter mass function (Press & Schechter 1974) with the modification of Sheth & Tormen (1999), expressed in units of (physical Mpc) $^{-3} M_{\odot}^{-1}$. In the vicinity of a massive halo dn/dM must be modified relative to the background universe. The dominant contribution to the modification of the halo mass function originates from the accelerated formation of halos in overdense regions. The calculation of this enhanced mass-function is described in Wyithe & Loeb (2005).

The quantity D_* in equation (A1) is the characteristic physical size of a spherical HII region generated by stars in a galaxy with a dark matter halo of mass M_{halo} , and was given by Loeb et al. (2005)

$$D_* = 0.75 \left(\frac{M_{\text{halo}}}{10^{10} M_{\odot}} \right)^{1/3} \left(\frac{f_* f_{\text{esc}} / N_{\text{reion}}}{0.003} \right)^{1/3} \times \left(\frac{N_*}{4000} \right)^{1/3} \left(\frac{1+z}{7.5} \right)^{-1} \text{Mpc}, \quad (\text{A2})$$

where f_* is the fraction of baryons in the halo that are turned into stars, and f_{esc} is the fraction of ionising photons that escape from the galaxy into the surrounding IGM. The number of ionising photons per baryon incorporated into Pop-II stars is $N_* \sim 4000$ (Bromm et al. 2001), and N_{reion} denotes the number of photons required per baryon for the reionisation of the HII region. The value of N_{reion} depends on the number of recombinations and hence on the clumpiness of the IGM.

When (equation A1) is substituted into Eq (7), the enhancement of ionising background at radius R can be computed. Several model parameters need to be specified: First of all, we take M_{\min} to correspond to $v_{\text{circ}} = 50 \text{ km s}^{-1}$, which reflects the fact that only galaxies more massive than this can form in an ionised IGM, and hence contribute to the ionising background. Furthermore, we have assumed the ionising photons' mean-free-path to be equal to the measured value at $z = 5.7$, $\lambda \sim 1 - 5 \text{ physical Mpc}$ (Fan et al. 2006). Last, we need to specify the precise dependence of D_* on halo mass, by specifying the product $f_* f_{\text{esc}} / N_{\text{reion}}$. These model parameters were chosen to achieve reionisation at $z = 6$ as in Wyithe & Loeb (2005).